Sains Malaysiana 51(4)(2022): 1271-1282
http://doi.org/10.17576/jsm-2022-5104-25

Analyzing Interferometric CO (3-2) Observations of NGC 4039

(Menganalisis Interferometrik CO (3-2) Pemerhatian NGC 4039)

JAZEEL H. AZEEZ[1,*], ZAMRI ZAINAL ABIDIN[2], SADEEM ABBAS FADHIL[1] & CHORNG-YUAN HWANG[3]

[1]*Al-Nahrain University, Faculty of Science, Physics Department, Baghdad 10072, Iraq*
[2]*Physics Department, Faculty of Science, University of Malaya, 50603 Kuala Lumpur, Federal Territory, Malaysia*
[3]*National Central University, Graduate Institute of Astronomy, Chung-Li, 32054, Taiwan*

Received: 12 August 2021/Accepted: 25 October 2021

ABSTRACT

Starburst merging galaxies are important in the history of galaxy evolution timeline. For this work, we have chosen the Antennae galaxy (NGC4039), which is one of the most famous starburst merging galaxies. We analyzed the CO (3–2) interferometric observations for the southern mosaic of the NGC 4039, together with the CO (2–1) data taken from Atacama Large Millimeter/Sub-millimeter Array (ALMA). Using the galactic CO luminosity to H_2 mass conversion factor, we found molecular gas mass range in this galaxy to be (0.8–2.92) × 10^8 $M_\odot$. Line emissions at CO (2–1) and CO (3–2) were detected at selected regions in the nucleus of NGC 4039. The CO (3–2) / CO (2–1) ratio for this galaxy was calculated to be approximately 0.62. In addition, we found a significant correlation between the brightness temperature ratio and IR luminosity for this galaxy. We used a new model to interpret the rotation curve and found that the most important factor is related to gas mass distribution. The disturbance in the gas distribution may be caused by the merging process. We have also analyzed the spatially resolved star formation law in this galaxy up to 345 parsec. We found a breakdown of the Kennicutt–Schmidt law at this scale. The results are consistent with the previous findings that there is a possibility of sub-thermally excited widespread gas in the neighborhood of denser regions, which causes the flatter star formation law.

Keywords: Galaxy evolution; NGC 4039; rotation curve; starburst; star formation

ABSTRAK

Galaksi percantuman ledakan bintang adalah penting dalam sejarah garis masa evolusi galaksi. Dalam kajian ini, kami memilih galaksi Antennae (NGC4039) yang merupakan salah satu galaksi percantuman ledakan bintang yang terkenal. Kami menganalisis hasil cerapan interferometer CO (3-2) bagi mozek selatan NGC4039, bersama-sama dengan data CO (2-1) yang diambil daripada Atacama Large Millimeter/Sub-millimeter Array (ALMA). Dengan menggunakan faktor penggubah kecerahan CO untuk galaksi kepada jisim H_2, kami mendapati bahawa julat jisim gas molekul adalah (0.8–2.92) × 10^8 $M_\odot$. Nisbah CO (3–2)/CO (2–1) untuk galaksi ini telah dihitung sebagai lebih kurang 0.62. Tambahan pula, kami mendapati hubungan ketara antara nisbah suhu kecerahan dan IR kelumenan bagi galaksi ini. Kami menggunakan suatu model baharu bagi menginterpretasi lengkung putaran dan mendapati bahawa faktor terpenting bagi model ini berkait dengan pembahagian jisim gas. Sebarang gangguan dalam pembahagian gas mungkin disebabkan oleh proses percantuman. Kami juga telah menganalisis hukum kejadian bintang reruang terlerai dalam galaksi ini sehingga 345 parsec. Kami mendapati hukum Kennicutt–Schmidt gagal pada skala ini. Keputusan kajian ini adalah tekal dengan keputusan sebelum ini yang berkemungkinan terdapat gas tersebar teruja secara sub-terma dalam kawasan kejiranan yang lebih padat dan ini akan menjadikan hukum kejadian bintang yang lebih rata.

Kata kunci: Evolusi galaksi; ledakan bintang; lengkuk putaran; NGC 4039; pembentukan bintang

INTRODUCTION

It is of essential significance in astronomy and astrophysics to understand the galaxy formation and evolution. The physical interaction in the merging galaxies represents an interesting phenomenon that gives an evidence on how galaxies evolve over time (Saviane et al. 2004).

Furthermore, the galactic mergers are accompanied with bursts of star formation that forms the building blocks of galaxies (Barnes & Hernquist 1992; Kennicutt et al. 1998; Larson 1990). Since galaxies are dominated by stars, the star formation is an intrinsic process in galactic formation and evolution. Stars are formed in dense cores of giant molecular clouds (GMCs), where the heavy elements and kinetic energy are released into the interstellar medium through supernova explosion. Thus, it is important to best understand the formation of GMC, the source of star formation in galaxies. Observations of GMCs made by millimeter CO emission lines enable us to investigate the molecular gas whose density is comparable or larger than 100 cm^{-3}. We know that the most considerable species, H_2, do not have proper line emission in sub-millimeter and millimeter regions because of its big separation between the lower levels of energy (~200 K), which are not excited sufficiently in the ideal physical conditions of molecular clouds (a few tens of Kelvin). New advances in sub-millimeter observation allow us to calculate physical parameters of molecular clouds. These sub-millimeter studies were carried out by many sub-millimeter telescopes. One of the newest and best telescopes is the Atacama Large Millimeter/Sub-millimeter Array (ALMA) which observe the molecular lines with frequency coverage approaching 800 GHz and even THz regime.

The Antennae galaxy (NGC 4038/9) is one of the nearest major merger galaxies that can be used to study the properties of molecular gas at high spatial resolution. The two progenitor spiral galaxies in this galaxy are initiated to merge about (400 - 600) × 10^6 years ago (Mihos et al. 1993; Teyssier et al. 2010). The interacting galaxies show luminous CO emission (Wei et al. 2012; Whitmore et al. 2014; Wilson et al. 2003) at each nucleus and in the overlap region, where the galaxies are colliding. In previous literatures, the Antennae galaxy has been studied at many wavelengths from radio to X-ray. Whitmore et al. (1999) observed the Antenna galaxy with Wide Field Planetary Camera 2 of the *Hubble Space Telescope* (*HST*) and they found many star clusters were created during the merging process. Neff and Ulvestad (2000) used Very Large Array (VLA) to observe 4 and 6 cm radio continuum emission and they measured that the total star formation rate (SFR) about 20 times larger than nearby spiral galaxies. Zhu et al. (2003) observed CO (1–0) using Nobeyoma 45 m telescope, and also they used CO (2–1) and CO (3–2) lines from James Clerk Maxwell Telescope to study CO (3–2)/CO (1–0) line ratio variations in the overlap region. In addition, Muders et al. (2007) determined CO line ratio which were less than that estimated by Zhu et al. (2003). Bigiel et al. (2015) combined millimeter data from the Combined Array for Research in Millimeter-wave Astronomy (CARMA) with infrared (IR) data from *Herschel* to estimate the star formation efficiency (SFR/H_2 α IR/CO) of dense gas and they found fundamental variation in the ratios of IR to the dense gas (IR/HCN) across the galaxy in terms of integrated intensities and the previously mentioned ratios. Recently, Matthews et al. (2018) utilized data from ALMA and *HST* to determine the ratio of stellar to gas mass (which is equivalent to the SFE) then they found that small number of clusters have SFE greater than 0.2, which indicates that a tiny part of these clusters stay bound.

NGC 4039 is a starburst galaxy colliding with a spiral galaxy NGC 4038. Understanding such type of galaxies is important to understand the galaxies evolution (Schirm et al. 2016; Ueda et al. 2017). The aim of this paper was to study the physical properties and the kinematic of CO (3–2) molecular gas in the southern mosaic of the Antennae galaxy, NGC 4039, at sub-kpc scale using high resolution archival ALMA data. This paper is organized as follows: We describe our observations in the next section. In Section 3, we provide a discussion of our results where we present the CO (3–2)/(2–1) brightness temperature ratio, the molecular gas masses, the kinematics in NGC 4039, and the relation between molecular gas mass density and star formation rate density. We summarize and conclude this paper in the final section.

Materials and Methods

ALMA data

The Antennae galaxy (NGC 4038/39) were observed in ^{12}CO (2-1) and ^{12}CO (3-2) line emissions using Atacama Large Millimetre/Sub-millimetre Array (ALMA) cycle-0 science verification data with band 6 (λ = 1.25 mm) and band 7 (λ = 0.87 mm) receivers. In this paper, we will use only the southern mosaic that refer to NGC 4039. This galaxy was observed on 28 May 2011 with a total integration time of 4927.1 s. The observation formed of 29 pointing mosaics centered at RA = $12^h\ 01^m\ 54.016^s$, Dec = $-18^\circ\ 53'\ 07.920''$. The data have rms of 2.94 Jy.km/s with a spectral resolution of 10 km/s. The observation parameters are listed in Table 1. The data were calibrated and imaged using Common Astronomy Software Applications package (CASA) version 4.1. The data were publically available at ALMA portal (http://bulk.cv.nrao.edu/almadata/sciver/Antennaeband7). The

CO (3-2) integrated intensity (moment 0) and velocity field (moment 1) maps are shown in Figure 1(a) and 1(b). Its worthy to mention that Ueda et al. (2012) used SMA data with restoring beam 1.42″ × 1.12″, while in the present work we used a high resolution ALMA data with restoring beam 1.08″ × 0.62″.

TABLE 1. ALMA observation parameters

Parameter	Value (band-7)
Target	NGC 4039
Observing date	28 May 2011
Total integration time	4927.1 s
Field center	
R.A. (J_{2000})	$12^h\ 01^m\ 54.016^s$
Dec. (J_{2000})	$-18^\circ\ 53'\ 07.920''$
Number of Antenna	11
Rest Frequency	345.79 GHz
Restoring beam	(Major, Minor, P.A.) (1.08″, 0.62″, 70.19°)
Integrated flux density	1658.98 Jy km/s
Total bandwidth	1.875 GHz
Total channels	3840
Velocity resolution	10 km/s
rms	2.94 Jy km/s

SPITZER DATA

The IR data are used as tracers of star formation. In this work, the IR data was obtained from the Multiband Imaging Photometer of Spitzer Space Telescope (MIPS) at 24 μm. *SPITZER* has a sensitivity that is three orders of magnitude more than that of any previous space-based and ground-based infrared observatory. The full width at half maximum (FWHM) of the MIPS maps point-spread function (PSF) at 24 μm is 6″. The 24 μm data has a ~5′ square field of view with a pixel size of 2.55″.

RESULTS AND DISCUSSION

CO LINE RATIO

In Figure 2, we overlaid the CO (2-1) moment-0 contours on the CO (3-2) image. The overall distribution for both CO (3-2) and CO (2-1) are very similar. We divided the southern mosaic into 10 regions (S1 - S10) following the same procedure in Azeez et al. (2018, 2016) covering the strong emission of CO as shown in Figure 2. Similar to Espada et al. (2012), we consider the regions from S1 - S6 within the overlap region. The region S7 will be considered within the molecular arm and the regions from S8-S10 are within the NGC 4039. The sizes of all boxes are equal to 2.5″ × 2.5″, which corresponds to 345 pc× 345 pc. The CO (3-2)/CO (2-1) brightness temperature ratio, R_{32}, are derived for each region. The positions, flux density and the brightness temperature ratio are listed in Table 2. R_{32} is less than 1 for all regions. It distributed in the range of 0.46 to 0.81 with an average value of 0.62 which is similar to the average value in the nuclei

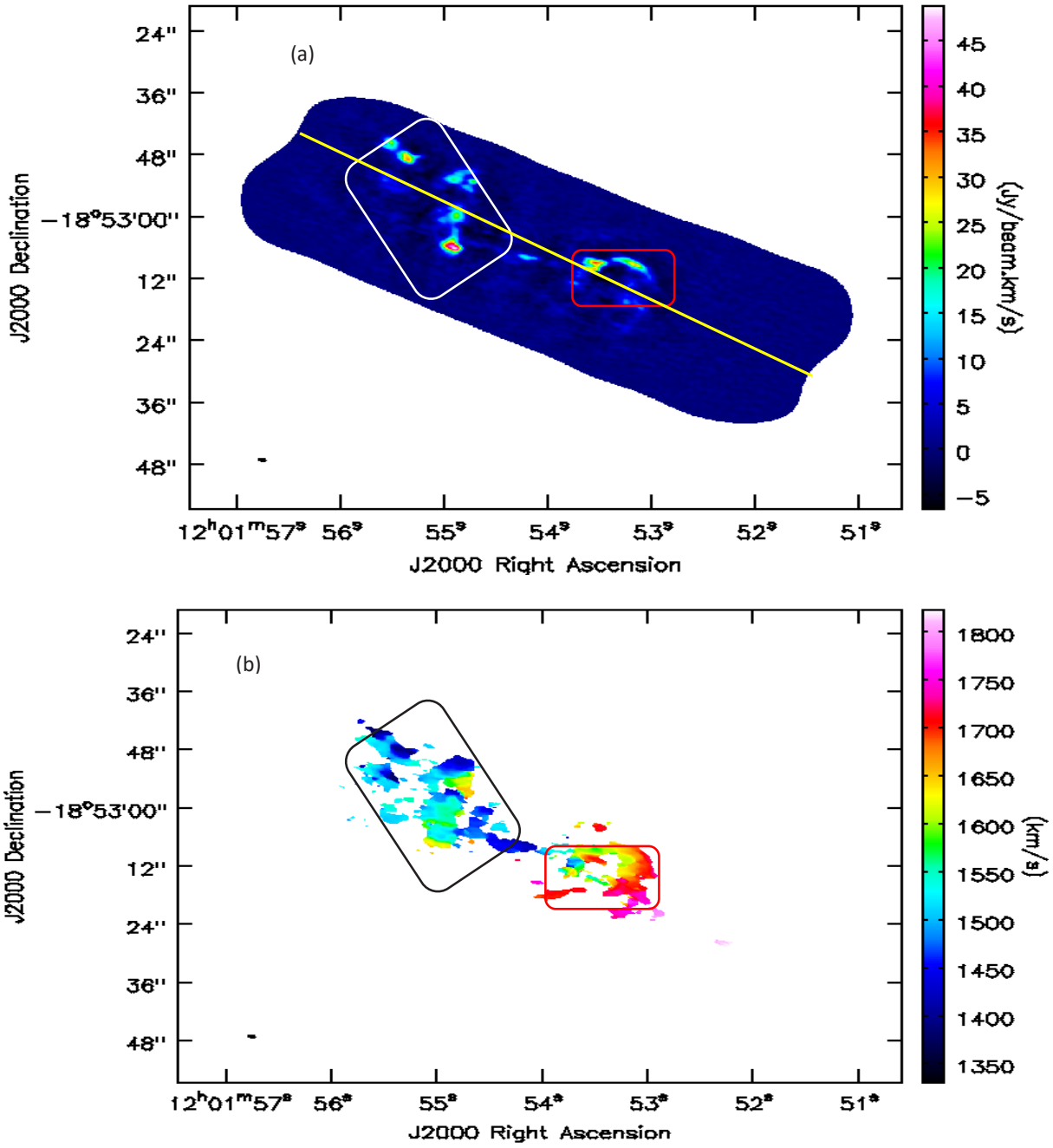

FIGURE 1. (a) CO (3-2) integrated intensity map (moment 0) of NGC 4039. The red square represents the nucleus of NGC 4039 and the white rectangular represent the overlap region. The Yellow line represent roughly estimated PV slice, (b) CO (3-2) velocity field map (moment 1) of NGC 4039. The red square represents the nucleus of NGC 4039 and the black rectangular represents the overlap region

of nearby starburst and spiral galaxies (Devereux et al. 1994; Mauersberger et al. 1999). We measured the strength of correlations between the R_{32} and CO line intensity using Pearson correlations as shown in Figure 3. We find that R_{32} correlates tightly with CO line intensities (the peak in CO is peak in R_{32}) with correlation coefficient

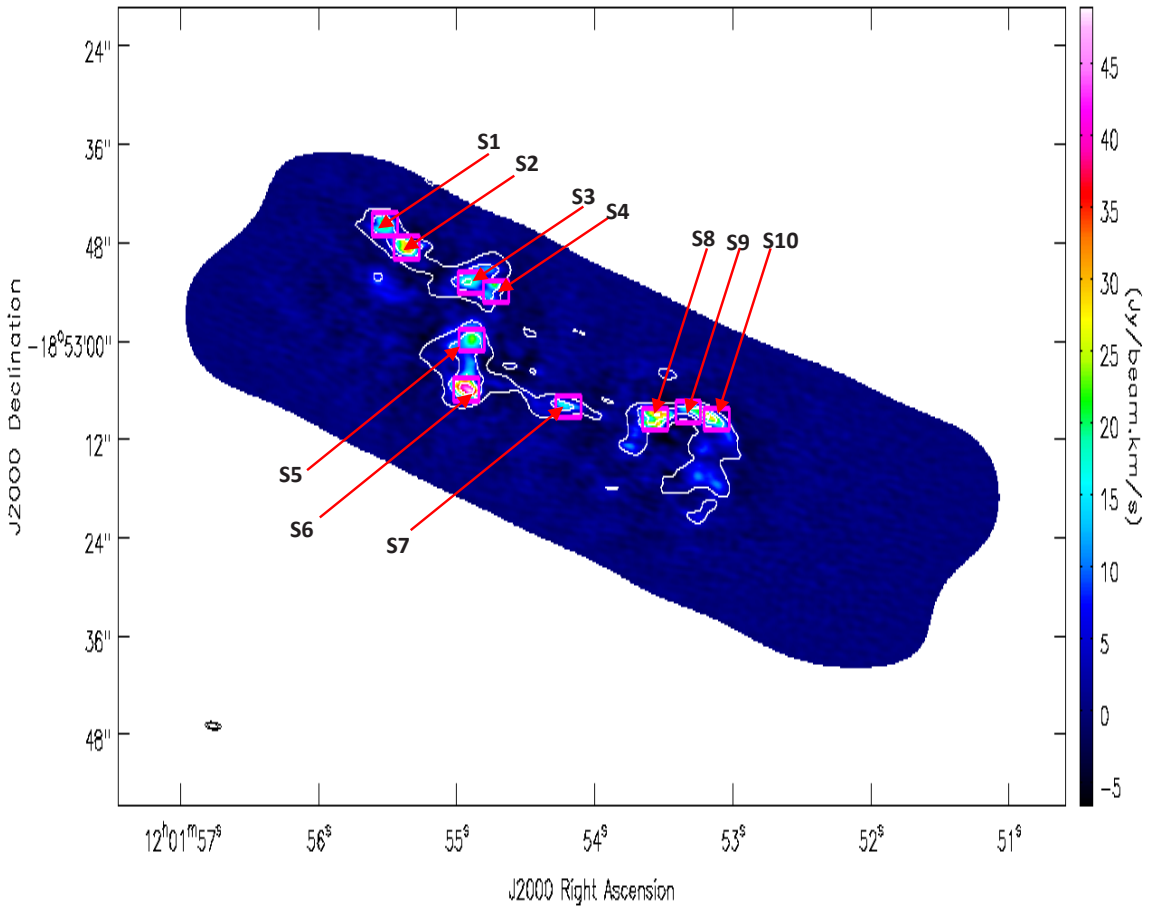

FIGURE 2. Integrated intensity maps of CO (2-1) (solid contours) overlaid on integrated intensity maps of CO (3-2) (raster image). Solid contour levels for CO (2-1) are 0.2, 0.4, 0.6 and 0.8 × 3.32 Jy . beam^{-1}. km . s^{-1}. We plot 10 boxes (S1–S10) to calculate the line ratios

r = 0.89 and probability of p = 99.5%, this fact suggests that R_{32} is sensitive to the density. The small increase in R_{32} versus CO line intensity indicates that both transitions CO (2-1) and CO (3-2) follow the same behaviour, may be due to increase of gas temperature or/and gas density that lead to excite more gas molecules and therefore increase these transitions.

MOLECULAR GAS MASS

The mass of the molecular gas in our sample can be estimated from ^{12}CO (3-2) luminosity using equations (1) and (2) (Rivera et al. 2018; Solomon & Bout 2005):

$$L'_{CO} = 3.25 \times 10^7 S_{CO}\Delta v\, \nu_{obs}^{-2}\, D_L^2 (1+z)^{-3} \qquad (1)$$

$$\left(\frac{M_{CO}}{M_\odot}\right) = \alpha_{CO} L'_{CO} \qquad (2)$$

where L_{CO}' in K km/s pc^2, S_{CO} Δv is the integrated flux in unit of Jy km/s, ν_{obs} is the observing frequency in unit of GHz, D_L is the luminosity distance in unit of Mpc. The CO-to-H_2 galactic conversion factor, α, will be used following the work of Bolatto et al. (2013) who reviewed several studies that are related to conversion factor in different galaxies and found the best value of α is 4.35. The ratio of I (3-2)/ I (1-0) is studied by Ueda et al. (2012) for Antenna galaxy. The best value found in the nucleus of NGC 4039 was about 0.77 and we have used this value in our calculations of equation (1). We did not correct by 1.36 to account for Helium. Using this conversion factor, the molecular gas mass range (0.8-2.92) × 10^8 $M_\odot$, this probable includes giant molecular cloud. The molecular gas mass surface density ranges from (0.52–2.5) × 10^3 $M_\odot$/pc^{-2}. The molecular gas mass and surface density for each individual box are listed in Table 3. The results

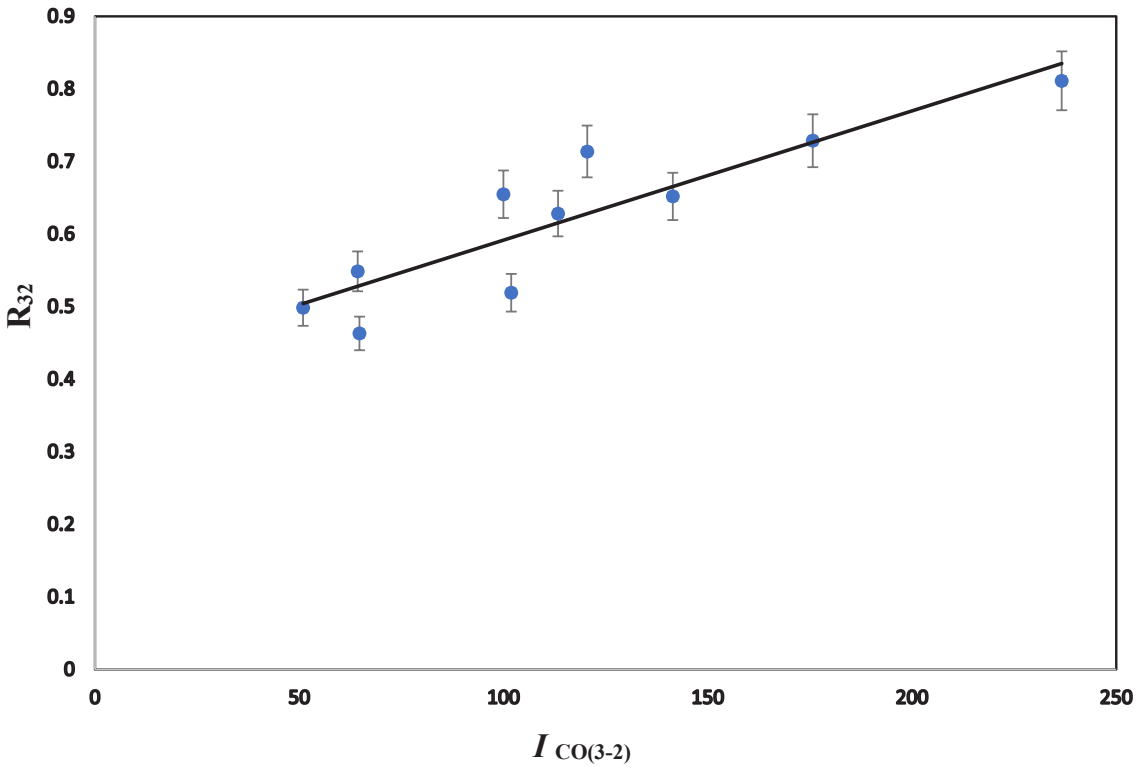

FIGURE 3. Comparison between the CO(3–2)/CO(2–1) integrated intensity ratio, R_{32}, and the CO line intensities ($I_{CO(3-2)}$). The error bars have included 5 percent of our integrated intensity ratio, R_{32}. The slope has a value of 0.0018

showed a relatively high gas mass in the regions 1-3, 5, 8, and 10. Most of these regions encounter high brightness temperature ratio, R_{32}, which may indicate that there are active collision processes happened within these regions. The high molecular gas mass agrees with such conditions.

TABLE 2. Integrated flux density of CO (3-2) and CO (2-1), right ascension, declination and brightness temperature ratio

Region	Right Ascension	Declination	$S_{CO(3-2)}\Delta V$ (Jy km/s)	$S_{CO(2-1)}\Delta V$ (Jy km/s)	R_{32}
S1	$12^h\ 01^m\ 55.517^s$	$-18^\circ\ 52'\ 45.482''$	100.59 ± 5.8	67.96 ± 5.4	0.66
S2	$12^h\ 01^m\ 55.362^s$	$-18^\circ\ 52'\ 48.382''$	142.37 ± 9.1	97.71 ± 8.4	0.65
S3	$12^h\ 01^m\ 54.897^s$	$-18^\circ\ 52'\ 52.598''$	101.62 ± 4.1	86.95 ± 4.4	0.52
S4	$12^h\ 01^m\ 54.717^s$	$-18^\circ\ 52'\ 53.793''$	64.85 ± 5.7	52.26 ± 8.0	0.55
S5	$12^h\ 01^m\ 54.889^s$	$-18^\circ\ 52'\ 59.697''$	120.79 ± 4.4	75.28 ± 6.4	0.71
S6	$12^h\ 01^m\ 54.931^s$	$-18^\circ\ 53'\ 05.712''$	237.75 ± 11.7	131.07 ± 9.6	0.81
S7	$12^h\ 01^m\ 54.192^s$	$-18^\circ\ 53'\ 07.718''$	50.53 ± 4.9	44.62 ± 5.6	0.50
S8	$12^h\ 01^m\ 53.559^s$	$-18^\circ\ 53'\ 09.343''$	176.21 ± 8.4	107.23 ± 8.2	0.73
S9	$12^h\ 01^m\ 53.323^s$	$-18^\circ\ 53'\ 08.395''$	65.52 ± 6.5	63.84 ± 9.1	0.46
S10	$12^h\ 01^m\ 53.142^s$	$-18^\circ\ 53'\ 09.343''$	113.79 ± 8.4	80.71 ± 10.4	0.63

CO (3-2) ROTATION CURVE

We used high resolution ALMA CO (3-2) data to find the rotation curve of NGC 4039. We derived the rotation curve from the position – velocity image (PV). We create the position velocity image using CASA task IMPV with start and end points (615.5, 226.1) and (98.4, 521.3), respectively. The PV diagram is showed in Figure 4. In spite of the PV diagram result from (Ueda et al. 2012) agreed with our result, but they did not study the rotation curve of this galaxy as we have done. To obtain the central rotation curve of this galaxy we used the following formula (3) (Azeez et al. 2021, 2015):

$$V_{rot} = \frac{|V_{obs} - V_{sys}|}{\sin(i)} \quad (3)$$

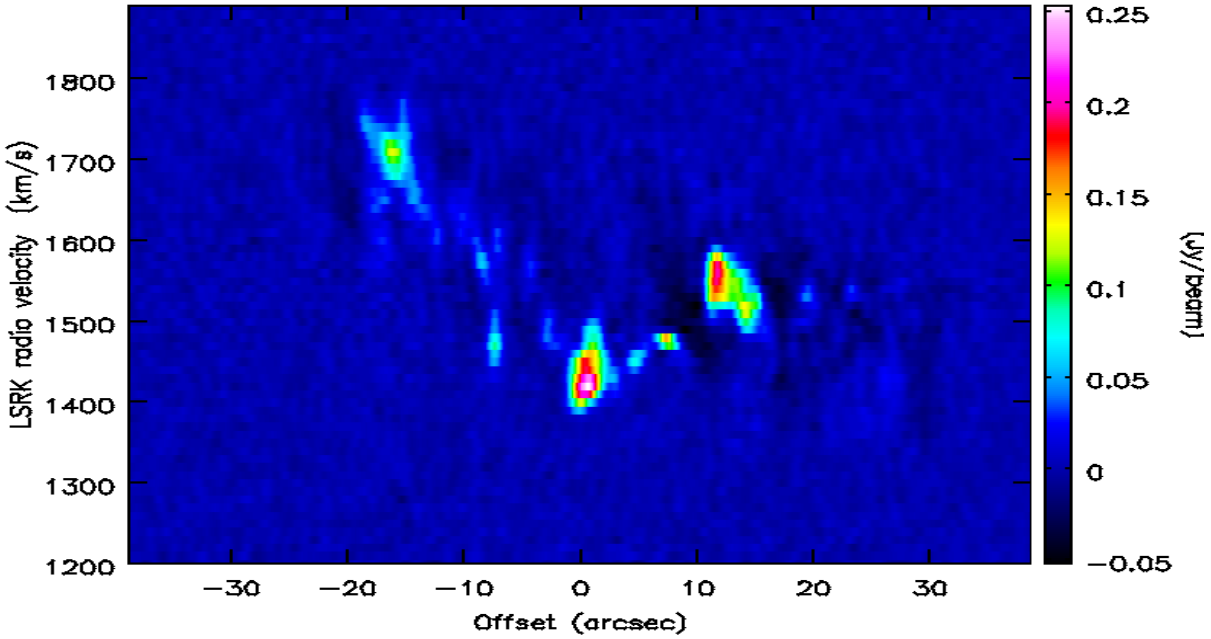

FIGURE 4. Position-Velocity diagrams of CO (3-2) emission in NGC 4039

where V_{sys} is the systematic velocity of the galaxy and i is the inclination angle of the galaxy. We used V_{sys}=1400 km/s from Karachentsev and Makarov (1996) and i = 60° following Ueda et al. (2012).

In Figure 5, we showed the rotation curve of NGC 4039. To interpret the rotation curve physically, we used a new fitting model that is based on a new theory called Time of Events Theory (Fadhil et al. 2021, 2020, 2014). The detailed model derivation will be published elsewhere. Fundamentally, this model follows the strategy of adopting the independent parameters for the rotation curve in galaxies, which are determined from the energy equation, then an equation is written in terms of these parameters with constants that are found from the experimental data. The three main parameters that the rotation curve is found to be dependent on are; 1) The gas mass distribution in the galaxy, 2) the gravitational attraction between different gas regions, and 3) the centrifugal acceleration. Ultimately, we found that v is related to r through equation (4) (details of the rotational velocity equation derivation, using the previously mentioned parameters, will be published elsewhere):

$$v \propto (r^3, r^{\frac{1}{2}}, \frac{1}{r}) \quad (4)$$

where r is the distance in kpc, the first parameter leads to the rotational velocity to be proportional to r^3, the second parameter leads to a proportionality with $r^{1/2}$, and the third parameter leads to a proportionality with $1/r$.

The final equation for the rotational velocity is concluded taking into account that these three terms may be found in action together in some regions, therefore the yielded equation will take into account such combination between different terms as in equation (5):

$$v = \alpha r^3 + \beta r^{1/2} + \gamma \frac{1}{r} + \delta r^{7/2} + \varepsilon r^2 + \epsilon \frac{1}{r^{1/2}} + \mu r^{5/2} + \sigma \quad (5)$$

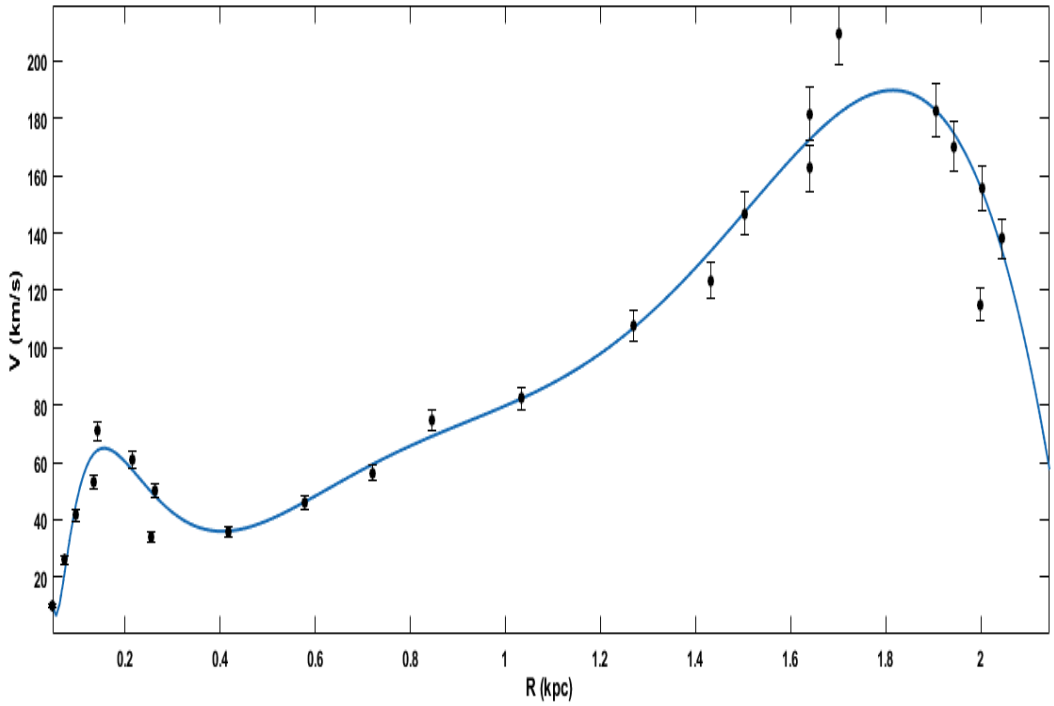

FIGURE 5. Rotation curve of CO (3-2) emission in NGC 4039 derived from PV diagram. Filled circle are the data points and the solid curve is the equation (5) fit

where $\alpha, \beta, \gamma, \delta, \varepsilon, \epsilon, \mu$ and σ are proportionality constants for the first term, second term, third term, combination between first and second term, combination between first and third term, combination between second and third term, the combination for the three terms together, and an offset fitting constant, respectively. A MATLAB program was written to accomplish the least square fitting for the experimental data using equation (5). The fitting results are listed in Table 3 and the fitting line is shown in Figure 5.

From Figure 5, it is clear that the fitting line matches well with the experimental data. The reduced Chi-squared test was performed to test the goodness of fit for the present model. The reduced Chi-squared parameter χ_{υ} was found to equal 0.55, which is around one. For astrophysics data, this is considered as a good result for a fitting model (Katz et al. 2017). The fitting constants in Table 3 showed that the mass distribution term has the largest effect on the rotational velocity, it should be mentioned here that the gas density is assumed constant within the galaxy, therefore the large value of such parameter refers to non-homogenous distribution for the gases in this galaxy. This may be due to the fact that this galaxy is merging within the galaxy. The second term which is the centrifugal acceleration term, has the second effect on the rotational velocity, while the third term, which is the gravitational attraction term, has the least value. This is expected because, on average, the gas is distributed with relatively low density within most regions in the galaxy. Other mutual interaction terms are usually having a value that lies between the values of their original terms' values, which is logical. Within the central 140 pc, the rotational velocity increased with radius, so the dynamical mass within this radius can be estimated, by equating the kinetic energy to the potential energy, from Newton's law of gravity, and solving for M, we get equation (6):

$$M = \frac{rV^2}{G} \tag{6}$$

where V is the rotation velocity at radius of the galaxy, r the radius of the gas disk, and G is the gravitational constant. The total mass inside 140 pc radius is 1.56×10^8 $M_{\odot}$.

TABLE 3. The fitting constants in equation (5) after making the least square fit for the experimental data

The Constant	Value (upper bound, lower bound)
α	3.097e+04 (1.204e+04, 4.991e+04)
β	-8068 (-1.351e+04, -2628)
γ	130 (28.54, 231.6)
δ	-7112 (-1.134e+04, -2883)
ε	2.783e+04 (1.004e+0, 4.561e+04)
ϵ	-1511 (-2611, -410.7)
μ	-4.808e+04 (-7.821e+04, -1.795e+04)
σ	5921 (1840, 1e+04)

STAR FORMATION LAW

We obtained the 24 μm IR image of NGC 4039 from the *Spitzer* archives. We used the 24 μm image to measure SFR using equation (7) (Azeez et al. 2017; Wu et al. 2005):

$$\frac{SFR}{[M_{\odot}yr^{-1}]} = \frac{v\,L_v[24\mu m]}{6.66\times10^{8}L_{\odot}} \qquad (7)$$

where L_v is the luminosity of 24 μm. In Table 4, we have combined important physical parameters for each region: the CO (3-2) integrated intensity obtained from ALMA data (Col. 2) molecular gas mass and surface density (Col. 3, 4), 24 μm luminosity derived from *Spitzer* data (Col. 5), SFR and SFR surface density (∑SFR), (Col. 6, 7), SFE as the ratio of 24 μm luminosity and molecular gas mass (Col. 8). The H_2 gas is considered as the fuel for star formation, therefore, it is suitable to trace the star formation process. As we mentioned earlier, the centre of NGC 4039 and the overlap regions are divided into 10 regions. We determined the surface densities of molecular gas $\sum H_2$ and star formation rate $\sum SFR$ in each region as shown in Figure 6(a). The slope of this figure represents the index of the power-law (Kenncuit-Schmidt law K-S law), which is also equivalent to the average star formation efficiency SFE, its value equal to 0.56 with intercept -1.86. We then measured the strength of correlations between these two variables using Pearson correlations and we found that there is a moderate correlation between $\sum H_2$ and $\sum SFR$ with correlation coefficient r = 0.48 and probability p = 88%. This suggests that the SF law breaks downs in this galaxy on scales of 345 pc. The very flat power-law slope caused $\sum H_2$ and $\sum SFR$ relation with index less than the Schmidt index of 1.4. This breakdown of the Kennicutt-Schmidt law cannot be interpreted by the model of Krumholz and Thompson (2007), which is a model that describes the dependence of K-S law on the molecular emission line used to trace the gas. We suggest that the considerable amounts of emission can yield from sub-thermally excited widespread gas in the neighbourhood of denser regions, which may cause a flatter star formation law as shown by Narayanan et al. (2008), who derived a physical model to interpret the SFL. From this model they concluded that lines having critical densities larger than the mean density of most emission clouds in a galaxy will have very little thermalized gas, resulting in a superlinear connection between molecular line luminosity and mean gas density. We also compare our results for NGC 4039, represented as red circles in Figure 6(b), with normal spiral galaxies and starburst galaxies of Kennicutt (Kennicutt et al. 1998). The $\sum SFRs$ for this galaxy are similar to the starburst galaxies, but higher than the normal galaxies. This result strongly upholds the idea that the inner region is undergoing a period of starburst (Tsai et al. 2012).

TABLE 4. CO (3-2) intensity, molecular gas density and mass, 24 μm Luminosity, star formation rate, star formation rate surface density, and star formation efficiency

Region	$S_{CO(3-2)}\Delta V$ (Jy km/s)	M(H_2) × 10^8 $M_\odot$	ΣH_2 ($M_\odot$ /pc)	$L_{24\,\mu m}$ × 10^8 $L_\odot$	SFR ($M_\odot$/yr)	ΣSFR ($M_\odot$/yr.kpc^2)	SFE ($L_\odot$/ $M_\odot$)
S1	100.59 ± 5.8	1.24	1038.80	0.66	0.10	0.85	0.53
S2	142.37 ± 9.1	1.75	1470.23	0.74	0.11	0.96	0.42
S3	101.62 ± 4.1	1.25	1049.43	0.61	0.09	0.78	0.49
S4	64.85 ± 5.7	0.80	669.66	0.61	0.09	0.79	0.77
S5	120.79 ± 4.4	1.48	1247.44	1.00	0.15	1.29	0.68
S6	237.75 ± 11.7	2.92	2455.26	2.50	0.38	3.21	0.85
S7	50.53 ± 4.9	0.62	521.86	0.58	0.09	0.74	0.93
S8	176.21 ± 8.4	2.17	1819.75	0.36	0.06	0.47	0.17
S9	65.52 ± 6.5	0.81	676.65	0.41	0.06	0.53	0.51
S10	113.79 ± 8.4	1.40	1175.10	0.36	0.06	0.47	0.26

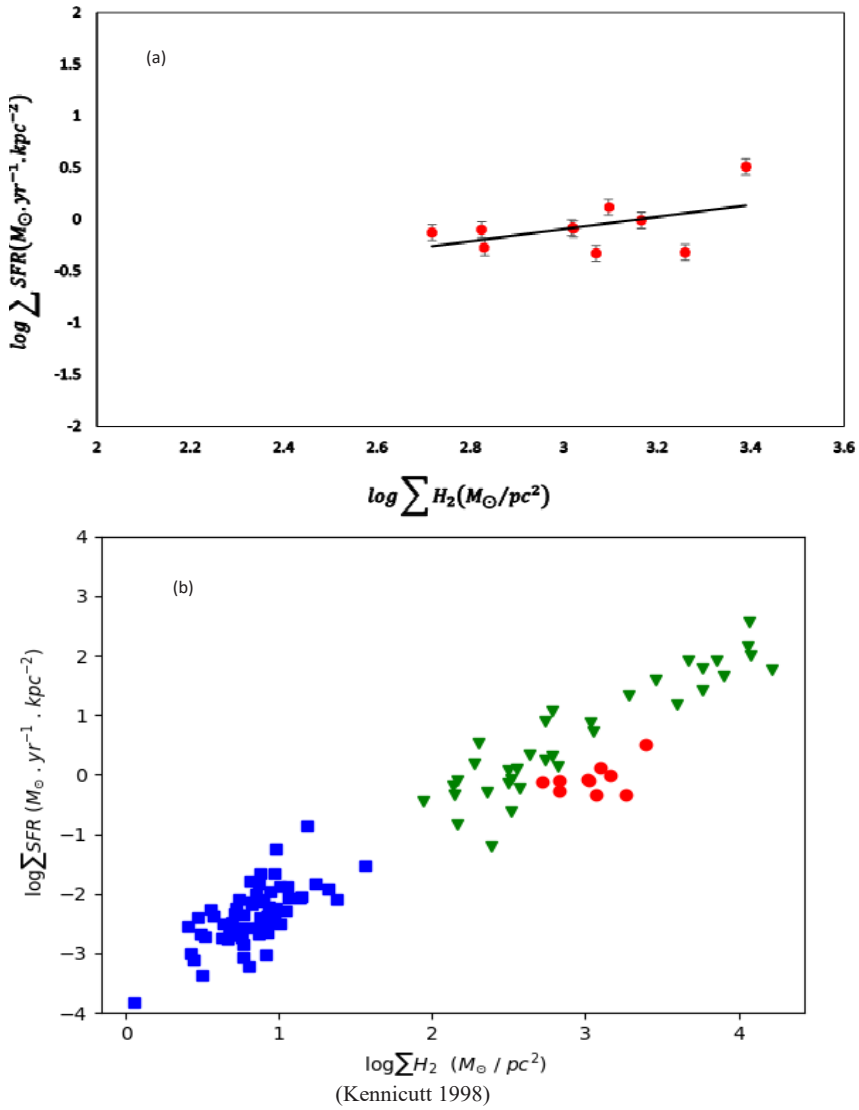

FIGURE 6. Relationship between (a) the molecular gas surface density and star formation rate surface density in NGC 4039 at 345 pc scale. (b) $\sum H_2$ and $\sum SFR$ for our sample NGC4039 (red circle), normal spiral galaxies (blue square) and starburst galaxies (green triangle) from Kennicutt (1988)

Conclusion

We analysed the interferometric CO (3–2) emission and compared it with CO (2-1) emission toward the southern mosaic (NGC 4039) of the Antenna galaxy obtained using ALMA at 345 pc scale. Both CO (3–2) and CO (2–1) emissions show similar distributions. We calculated the brightness temperature ratio, R_{32}, in different regions. We concluded that this ratio is significantly correlated with the CO line intensity because R_{32} is sensitive to the density. The physics behind such behavior is well known to be due to collisions that are proportional to the gas density. If there are an increment of collisions between gas molecules, their temperatures will also see an increment, and therefore increases the transitions of (3-2) relative to (2-1). In addition, this ratio is well correlated with IR luminosity, which indicates that the excitation regions are associated with warm gas/dust. The regions of high R_{32} ratio can be summarised to lie in the upper and lower parts of the overlapping regions, which are undergoing active gas collisions with the neighbourhood parts of the north and south galaxies, respectively. The nucleus of NGC 4039 also has high R_{32} ratio due to the observed high molecular emissions. The rotation curve fitting showed that the most effective term on the rotational velocity is the mass distribution term, which is due to the fact that this galaxy is merging with other galaxy that may lead to disturbance in its gas distribution. We also found a moderate correlation between $\sum H_2$ and $\sum SFR$ which suggests a breakdown for KS law at 345 pc scale due to sub thermal diffuse excited gas.

Acknowledgements

This paper makes use of the following ALMA data: ADS/JAO.ALMA# 2011.0.00004.SV. The Author ZZA would like to thank University of Malaya for their financial support (FG033-17 AFR).

References

Azeez, J.H., Zghair, A.A., Fadhil, S.A. & Abidin, Z.Z. 2021. Rotational velocity and dynamical mass for the nuclear disk of the ULIRG Arp 220. *Journal of Physics: Conference Series* 1829: 012004.

Azeez, J.H., Fadhil, S.A., Naser-Alla, Z.K. & Abidin, Z.Z. 2018. ALMA study of the lensed galaxy SDP.81. *Al-Nahrain Journal of Science* 1: 69-71.

Azeez, J.H., Abidin, Z.Z., Hwang, C.Y. & Ibrahim, Z.A. 2017. Star formation law at sub-kpc scale in the elliptical galaxy Centaurus A as seen by ALMA. *Advances in Astronomy* 2017: 8416945.

Azeez, J.H., Hwang, C.Y., Abidin, Z.Z. & Ibrahim, Z.A. 2016. Kennicutt-Schmidt Law in the central region of NGC 4321 as seen by ALMA. *Scientific Reports* 6: 26896.

Azeez, J.H., Abidin, Z.Z., Ibrahim, Z.A. & Hwang, C.Y. 2015. Rotation curve and dynamical mass in the inner region of M100 with ALMA. *2015 International Conference on Space Science and Communication (IconSpace)*. IEEE. pp. 329-334.

Barnes, J.E. & Hernquist, L. 1992. Formation of dwarf galaxies in tidal tails. *Nature* 360: 715-717.

Bigiel, F., Leroy, A.K., Blitz, L., Bolatto, A.D., Cunha, E.D., Rosolowsky, E., Sandstrom, K. & Usero, A. 2015. Dense gas fraction and star formation efficiency variations in the Antennae Galaxies. *Astrophysical Journal* 815: 103.

Bolatto, A.D., Wolfire, M. & Leroy, A.K. 2013. The CO-to-H2 conversion factor. *Annual Review of Astronomy and Astrophysics* 51: 207-268.

Devereux, N., Taniguchi, Y., Sanders, D.B., Nakai, N. & Young, J.S. 1994. ^{12}CO (3-2) & (1-0) Emission line observations of nearby starburst galaxy nuclei. *The Astronomical Journal* 107(6): 2006-2016.

Espada, D., Komugi, S., Muller, E., Nakanishi, K., Saito, M., Tatematsu, K., Iguchi, S., Hasehawa, T., Mizuno, N., Iono, D., Matsushita, S., Trejo, A., Chapillon, E., Takahashi, S., Su, Y.N., Kawamura, A., Akiyama, E., Iraatsi, M., Nagai, H., Miura, R.E., Jurono, Y., Sawada, T., Higuchi, A.E., Tachihara, K., Saigo, K. & Kamazaki, T. 2012. Giant molecular clouds and star formation in the tidal molecular arm of NGC4039. *Astrophysical Journal Letters* 760(2): 1-5.

Fadhil, S.A., Azeez, J.H. & Hassan, M.A. 2021. Derivation of a new multiscale model: I. Derivation of the model for the atomic, molecular and nano material scales. *Indian Journal of Physics* 95(2): 209-217.

Fadhil, S.A., Hassan, M.A., Azeez, J.H. & Majeed, M.S. 2020. Derivation of a new multiscale model: II. deriving a modified hall-petch relation from the multiscale model and testing it for nano, micro, and macro materials. In *3rd International Conference on Sustainable Engineering Techniques (ICSET 2020)*. IOP Publishing 881: 01298.

Fadhil, S.A., Azeez, J.H. & Whahaeb, A.F. 2014. Solving the instantaneous response paradox of entangled particles using the time of events theory. *The European Physical Journal Plus* 129(23): 1-10.

Karachentsev, I.D. & Makarov, D.A. 1996. The galaxy motion relative to nearby galaxies and the local velocity field. *The Astronomical Journal* 111: 794-803.

Katz, H., Lelli, F., McGaugh, S.S., Di Cintio, A., Brook, C.B. & Schombert, J.M. 2017. Testing feedback-modified dark matter haloes with galaxy rotation curves: Estimation of halo parameters and consistency with ΛCDM scaling relations. *Monthly Notices of the Royal Astronomical Society* 466(2): 1648-1668.

Kennicutt, J.R.C. 1998. The global Schmidt law in star-forming galaxies. *The Astrophysical Journal* 498(2): 541-552.

Kennicutt, J.R.C., Schweizer, F., Barnes, J.E., Friedli, D., Martinet, L. & Pfenniger, D. 1998. *Galaxies: Interactions and Induced Star Formation.* Berlin: Springer. pp. 1-406.

Krumholz, M.R. & Thompson, T.A. 2007. The relationship between molecular gas tracers and Kennicutt-Schmidt Laws. *The Astrophysical Journal* 669(1): 289-298.

Larson, R.B. 1990. Formation of Star Clusters. In *Physical Processes in Fragmentation and Star Formation*, edited by Capuzzo-Dolcetta, R., Chiosi, C. & Fazio, A.D. Dordrecht: Springer Netherlands. pp. 389-400.

Matthews, A.M., Johnson, K.E., Whitmore, B.C., Brogan, C.L., Leroy, A.K. & Indebetouw, R. 2018. Resolved star formation efficiency in the Antennae galaxies. *The Astrophysical Journal* 862(2): 147).

Mauersberger, R., Henkel, C., Walsh, W. & Schulz, A. 1999. Dense gas in nearby galaxies XII. A survey for CO J = 3 − 2 emission. *Astronomy & Astrophysics* 341: 256-263.

Mihos, J.C., Bothun, G.D. & Richstone, D.O. 1993. Modeling the spatial distribution of star formation in interacting disk galaxies. *The Astrophysical Journal* 418(1): 82-99.

Muders, D., Schulz, A., Mauersberger, R., Mao, R.Q., Henkel, C. & Röllig, M. 2007. The interstellar medium of the Antennae galaxies. *Astronomy & Astrophysics* 466(2): 467-479.

Narayanan, D., Cox, T.J., Shirley, Y., Davé, R., Hernquist, L. & Walker, C.K. 2008. Molecular star formation rate indicators in galaxies. *The Astrophysical Journal* 684(2): 996-1008.

Neff, S.G. & Ulvestad, J.S. 2000. VLA observations of the nearby merger NGC 4038/4039: H II regions and supernova remnants in the 'Antennae'. *The Astronomical Journal* 120(2): 670-696.

Rivera, G.C., Hodge, J.A., Smail, I., Swinbank, A.M., Weiß, A., Wardlow, J.L., Walter, F., Rybak, M., Chen, C. & Brandt, W.N. 2018. Resolving the ISM at the peak of cosmic star formation with ALMA - The distribution of CO and dust continuum in Z~2.5 sub-millimetre galaxies. *The Astrophysical Journal* 863(1): 56.

Saviane, I., Hibbard, J.E. & Rich, R.M. 2004. The stellar content of the Southern Tail of NGC 4038/4039 and a revised distance. *The Astronomical Journal* 127(2): 660-678.

Schirm, M.R., Wilson, C.D., Madden, S.C. & Clements, D.L. 2016. The dense gas in the largest molecular complexes of the antennae: HCN and HCO+ observations of NGC 4038/39 using ALMA. *The Astrophysical Journal* 823(2): 87.

Solomon, P.M. & Vanden, B.P.A. 2005. Molecular gas at high redshift. *Annual Review of Astronomy and Astrophysics* 43: 677-725.

Teyssier, R., Chapon, D. & Bournaud, F. 2010. The driving mechanism of starbursts in galaxy mergers. *The Astrophysical Journal Letters* 720(2): L149.

Tsai, M., Hwang, C.Y., Matsushita, S., Baker, A.J. & Espada, D. 2012. Interferometric CO(32) observations toward the central region of NGC1068. *Astrophysical Journal* 746: 129.

Ueda, J., Iono, D., Petitpas, G., Yun, M.S., Ho, P.T.P., Kawabe, R., Mao, R.Q., Martin, S., Matsushita, S., Peck, A.B., Tamura, Y., Wang, J., Wang, Z., Wilson, C.D. & Zhang, Q. 2012. Unveiling the physical properties and kinematics of molecular gas in the Antennae galaxies (NGC4038/9) through high-resolution CO (J = 3-2) observations. *The Astrophysical Journal* 745: 65.

Ueda, J., Watanabe, Y., Iono, D., Wilner, D.J., Fazio, G.G., Ohashi, S., Kawabe, R., Saito, T. & Komugi, S. 2017. ALMA observations of the dense and shocked gas in the nuclear region of NGC 4038 (Antennae galaxies). *Publications of the Astronomical Society of Japan* 69(1): 1-9.

Wei, L.H., Keto, E. & Ho, L.C. 2012. Two populations of molecular clouds in the Antennae galaxies. *The Astrophysical Journal* 750: 136.

Whitmore, B.C., Brogan, C., Chandar, R., Evans, A., Hibbard, J., Johnson, K., Leroy, A., Privon, G., Remijan, A. & Sheth, K. 2014. ALMA observations of the Antennae galaxies. I. A new window on a prototypical merger. *The Astrophysical Journal* 795: 156.

Whitmore, B.C., Zhang, Q., Leitherer, C., Fall, S.M., Schweizer, F. & Miller, B.W. 1999. The luminosity function of young star clusters in 'the Antennae' galaxies (NGC 4038/4039). *The Astronomical Journal* 118(4): 1551-1576.

Wilson, C.D., Scoville, N., Madden, S.C. & Charmandaris, V. 2003. The mass function of supergiant molecular complexes and implications for forming young massive star clusters in the Antennae (NGC 4038/4039). *The Astrophysical Journal* 599(2): 1049-1066.

Wu, H., Cao, C., Hao, C.N., Liu, F.S., Wang, J.L., Xia, X.Y., Deng, Z.G. & Young, C.K.S. 2005. PAH and mid-infrared luminosities as measures of star formation rate InSpitzerFirst look survey galaxies. *The Astrophysical Journal* 632(2): L79-82.

Zhu, M., Seaquist, E.R. & Kuno, N. 2003. A multitransition CO study of the Antennae galaxies NGC 4038/9. *The Astrophysical Journal* 588(1): 243-263.

*Corresponding author; email: jazeelhussein@yahoo.com